

# Modeling the Effects of Microencapsulation on the Electro-Optic Behavior of Polymer Cholesteric Liquid Crystal Flakes

## Introduction

Polymer cholesteric liquid crystal (PCLC) flakes are micro-meter-scale platelets of PCLC material either generated by freeze fracturing of well-aligned, environmentally robust macroscopic PCLC films or formed in controlled shapes and sizes by means of a number of photolithographic, molding, or stamping techniques (Fig. 118.28).<sup>1-3</sup> Both processes rely on shear stress applied to the PCLC material surface during film or particle formation to align the helical molecular structure normal to the film surface. The unique temperature stability and optical properties of the parent films are preserved.

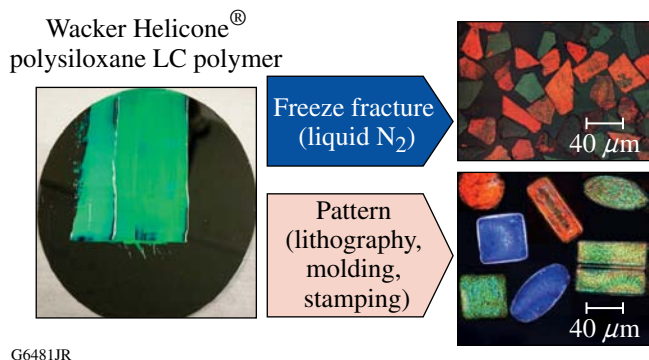


Figure 118.28

Methods for forming PCLC flakes from well-aligned parent films [blade-coated film on a 4-in.-diam polished silicon wafer (left), freeze fractured into flakes (top right)] or from shaped flakes made by soft lithography (bottom right).

First developed in the 1990s for passive optical applications, PCLC flakes display a Bragg-like (selective) reflection effect, where incident light of a specific wavelength and (circular) polarization component is strongly reflected from the flake to produce highly saturated, circularly polarized colors.<sup>1</sup> “Selective reflection” occurs when the incident light satisfies the condition  $\lambda = \bar{n}p$ , where  $\bar{n}$  and  $p$  are the average refractive index and the helical pitch length, respectively, of the PCLC material. This selective reflection is caused by the helical structure inherent to the PCLC material and can be designed to reflect either left- or right-handed circularly polarized light, depending on the

molecular structure of the PCLC polymers from which they are comprised. The individual color states depend on the flake’s helical pitch length, which may be tuned from the deep UV (nanometer-scale) to the IR (micrometer-scale) region, including the entire visible spectrum. The polymeric structure effectively “locks in” the helical pitch, making the selective reflection colors insensitive to temperature over a very broad temperature range.

## 1. Application of PCLC Flakes to Switchable Particle Devices

Switchable particle-based technologies are of increasing interest for a number of applications as industry looks to develop products with unique optical properties and capabilities. An obvious application for reflective particles is information displays that require low power consumption and high brightness. As a result of their intrinsic selective reflection, PCLC flakes can provide bright, saturated colors without the need for additional color filters and polarizers.<sup>4</sup> Composite PCLC flake systems composed of either stacked left- and right-handed PCLC materials, or a half-wave-plate material sandwiched between two materials of the same handedness, can potentially lead to particle displays with reflectivities exceeding 80% (Ref. 5). A PCLC particle display does not require backlighting in daytime light conditions and would be uniquely suited for point-of-sale devices, portable devices, and flexible media on either flat or curved surfaces (e.g., large-area signs, automobile dashboards, heads-up displays, and electronic paper). Other potential applications include switchable and tunable devices for color manipulation (i.e., switchable or tunable color filters); switchable and tunable optical retarders or modulators for polarized light at desired wavelengths or bandwidths; switchable micropolarizers; switchable “smart windows” for either energy or privacy control; switchable coatings for use in decorative applications; and switchable coatings for applications in military security, camouflage, substrate reflectance control, document security, anticounterfeiting, and object tagging or identification.<sup>6</sup>

## 2. Electro-Optical Behavior of PCLC Flakes

Kosc *et al.* were the first to investigate the switchable behavior of irregularly shaped PCLC flakes in an applied electric field.<sup>7-10</sup> When flakes in an appropriate host fluid are subjected

to an ac electric field, flake reorientation occurs as a result of Maxwell–Wagner (MW) interfacial polarization. Charges accumulate at the interface of the flake and the fluid, inducing a dipole on the flake. The applied electric field then acts on that dipole to reorient the flake parallel to the electric field. Interfacial polarization is driven by the difference between the flake and fluid dielectric constants and conductivities. Devices containing these “polarizing pigments” suspended in a commodity dielectric host fluid (e.g., silicone oil) at concentrations ranging from 3 wt% to 5 wt% switch rapidly ( $<1$  s) at very low voltages ( $10$  to  $100$   $\text{mV}_{\text{rms}}/\mu\text{m}$ ) (Refs. 4 and 11). Figure 118.29 shows the electric field–induced behavior of a PCLC flake/host fluid suspension in a typical, sandwich-cell geometry.<sup>9,12</sup> Figure 118.29(a) indicates the dimensions of the rectangular-shaped, 3:1-aspect-ratio polysiloxane PCLC flakes used for the work reported here.<sup>2</sup> With no field applied, the flakes lie nearly

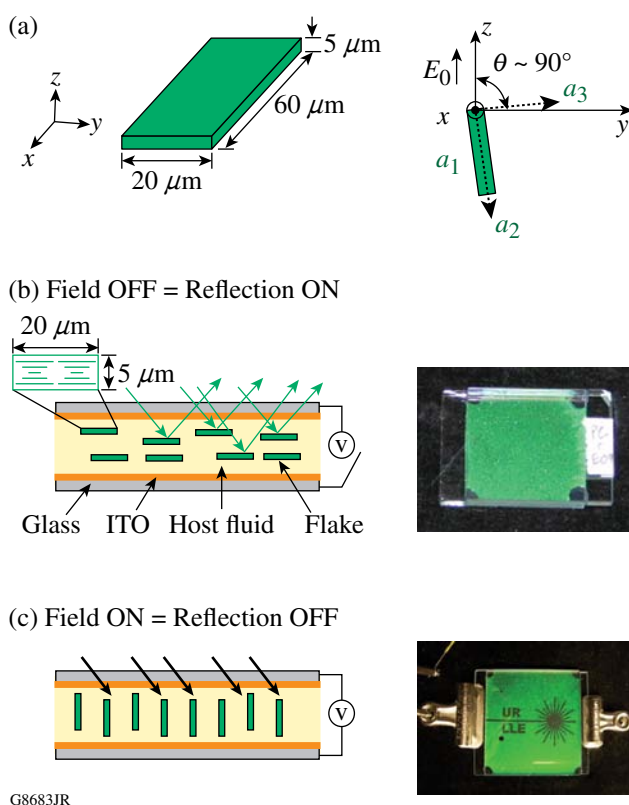


Figure 118.29

(a) Dimensions and coordinate system of a shaped PCLC flake. (b) Flakes lie approximately parallel to the cell substrates when no electric field is applied and appear colored as a result of selective reflection caused by the helical molecular structure of cholesteric liquid crystals, as depicted by the enlarged cross-sectional view of a flake. The longest axis is drawn into the page. (c) Flakes reorient with one long axis parallel to the applied field. As viewed from the incident light direction, rotated flakes appear dark since light is absorbed by the black back plane.

parallel to the substrates and selectively reflect one circularly polarized component of the incident light. An electric field applied to patterned electrodes produces flake reorientation by MW polarization and extinguishes the selective reflection color exposing the black back plane of the device [Fig. 118.29(c)]. The angle of rotation can range from  $\sim 10^\circ$  to  $90^\circ$ , depending on the dielectric constant and conductivity of both the flakes and the host fluid;  $15^\circ$  of rotation is often sufficient to extinguish the reflectivity.

Trajkovska-Petkoska *et al.* extended this work to shaped flakes, layered flakes, and doped flakes.<sup>3,13,14</sup> Uniformly shaped flakes lead to more-uniform reorientation times in an applied electric field. When the difference between host and flake conductivities is increased by doping, faster reorientation times attributable to both rotational and translational motion in a dc regime are observed. A combination of translational and rotational motion is observed when the dopant is not uniformly distributed throughout the particle. In moderately conductive hosts,  $90^\circ$  flake orientation is observed in the dc regime. Trajkovska-Petkoska *et al.* also expanded upon the original reorientation time model developed by Kosci *et al.* by including a gravity term for modeling flake relaxation times upon removal of the electric field.<sup>13,15</sup> This expanded analytical model was used for the calculations presented here.

### 3. Microencapsulation of PCLC Flake/Fluid Host Suspensions

For PCLC flakes to achieve their potential in many switchable particle device applications, high-volume and low-cost manufacturing techniques such as roll-to-roll processing can be developed by microencapsulation.<sup>16–23</sup> Microencapsulation as applied to PCLC flakes involves suspending the PCLC flakes in a host fluid and then encapsulating this flake/host fluid suspension by either (1) forming discrete, optically transparent shells (capsules) from a dilute polymer encapsulation medium that can in turn be dispersed into the body of a film-forming transparent polymer or (2) emulsifying the suspension directly into the body of the film-forming polymer to form discrete capsules. Microencapsulation is necessary to prevent flake migration or agglomeration and to allow one to apply the flake/host fluid system to any surface (rigid, flexible, or curved). Application may take place by a number of means, including knife coating, die coating, roll coating, and printing via ink-jet techniques.

In this work, we report on a method to model and predict the electro-optic (EO) behavior of microencapsulated, shaped PCLC flakes. Experimental results are presented to confirm the validity of the modeling as a tool for developing systems for switchable-device applications.

**Modeling and Devices**

1. Materials Systems

The materials used in this work were chosen for a number of compelling reasons. All the materials selected are available commercially in large quantities and at low cost and are essentially nontoxic. The host fluids were chosen to span a wide range of dielectric constants and conductivities to include a range of small to large electric-field interactions. Both the aqueous and nonaqueous polymer binder solutions employed in this work are easily emulsified and cast with standard laboratory equipment. The photoresist and UV-curable epoxy were selected because of their resistance to the chosen host fluids and their ability to be processed with standard laboratory equipment. The materials used in this work and their properties are listed in Table 118.II.

2. Modeling Methodology

The electric field that acts directly on the PCLC flake influences its EO behavior. In an ac electric field, the strength of the rotational torque applied to the flake depends on

1. the effective electric-field strength acting on the flake
2. the strength of the MW polarization induced on the flake surface, which is controlled by
  - a. the difference between the dielectric constants of the flake and host fluid
  - b. the difference between the conductivities of the flake and host fluid

When a dc field is applied, the EO behavior results from either MW polarization or electrophoresis. The dominating effect will depend on

1. the intrinsic charge on the flake in the host fluid
2. the strength of MW polarization induced on the flake surface by the difference between the dielectric constants of the flake and host fluid
3. the effective strength of the electric field acting on the flake

The rotational reorientation of a PCLC flake is the result of a balance of torques applied to the flake.<sup>13,15</sup> The electrostatic torque  $\Gamma_E$  from the applied electric field acts to reorient the flake as shown when moving from the “field OFF” state [Fig. 118.29(b)] to the “field ON” state [Fig. 118.29(c)]. The resistance to rotation is the sum of the torques caused by the hydrodynamic force ( $\Gamma_H$ ) and gravity ( $\Gamma_G$ ):

$$\Gamma_E = \Gamma_H + \Gamma_G. \tag{1}$$

The Clausius–Mosotti factor ( $K_i^*$ ) is a measure of the strength of the effective polarization of the flake. This factor incorporates the dielectric constant and conductivity of both the PCLC flake ( $\epsilon_p, \sigma_p$ ) and host fluid ( $\epsilon_h, \sigma_h$ ), the depolarization factor of the flake ( $A_i$ ), and the frequency of the applied electric field ( $\omega$ ):

Table 118.II: Properties of materials used for modeling and/or experiments.

Material	$\epsilon$	$\sigma$ (S/m)	$\rho$ (kg/m <sup>3</sup> )	$\eta_0$ (mPa • s)	Function
PCLC flakes*	2.2	$1 \times 10^{-9}$	1100	n/m	Particle
SIT7757	2.7	$3 \times 10^{-8}$	1070	35	Host fluid
DMS-E09	7.0	$9 \times 10^{-8}$	995	9	Host fluid
Propylene carbonate	60.0	$1 \times 10^{-4}$	1200	2	Host fluid
SU-8 3050 photoresist	3.2	$2.13 \times 10^{-8}$	n/m	n/a	Well/cube (walls)
SU-8 2015 photoresist	3.2	$2.13 \times 10^{-8}$	n/m	n/a	Cube (top/bot)
OG142-13 UV epoxy	6.9	$2.8 \times 10^{-7}$	n/m	n/a	Adhesive
PVA	2.0	$1 \times 10^{-9}$	n/m	n/a	Binder
Porcine gelatin	5.4	$1.79 \times 10^{-6}$	n/m	n/a	Capsule shell
Gum arabic	6.5	$1.08 \times 10^{-4}$	n/m	n/a	Capsule shell
PDMS	2.6	$1 \times 10^{-9}$	1030	n/a	Binder

n/m = not measured

n/a = not applicable

\*flake:  $L \times H \times D = 20 \times 5 \times 60 \mu\text{m}$

$$K_i^* = \frac{\left(\epsilon_p - i\frac{\sigma_p}{\omega}\right) - \left(\epsilon_h - i\frac{\sigma_h}{\omega}\right)}{\left(\epsilon_h - i\frac{\sigma_h}{\omega}\right) + A_i \left[\left(\epsilon_p - i\frac{\sigma_p}{\omega}\right) - \left(\epsilon_h - i\frac{\sigma_h}{\omega}\right)\right]}. \quad (2)$$

The electrostatic torque that drives flake reorientation may be written as a function of the flake's semi-axes ( $a_i$ ,  $a_j$ , and  $a_k$ ), the dielectric constant of the host fluid ( $\epsilon_h$ ), the imaginary portion of the Clausius–Mosotti factor ( $K_i^*$ ), the depolarization factor of the flake ( $A_j$ ), the strength of the electric field applied to the flake ( $E_0$ ), and the angle of the flake ( $\theta$ ) relative to the electric field:

$$\begin{aligned} \Gamma_{Ei} &= \frac{4}{3} \pi a_i a_j a_k \epsilon_h K_j^* K_k^* (A_k - A_j) E_0^2 \sin \theta \cos \theta \\ &= C_{Ei} \sin \theta \cos \theta. \end{aligned} \quad (3)$$

The hydrodynamic torque ( $\Gamma_{Hi}$ ) counteracts the electrostatic torque and may be defined as

$$\Gamma_{Hi} = \frac{16}{3} \pi a_i a_j a_k \eta_0 \frac{(a_j^2 + a_k^2)}{(a_j^2 A_j + a_k^2 A_k)} \Omega_i = C_{Hi} \Omega_i, \quad (4)$$

where  $a_i$  is the length of the flake semi-axes,  $\eta_0$  is the host fluid viscosity,  $A_j$  is the depolarization factor of the flake, and  $\Omega_i$  is the angular velocity of the flake about its axis. The torque caused by gravity ( $\Gamma_{Gi}$ ) is specific to the configuration in which the experiments are conducted. In this work the test devices lie flat and the force of gravity acts in the  $-z$  direction [Fig. 118.29(a)]. The gravitational torque is a function of the PCLC flake volume ( $V_p$ ), density of both the flake ( $\rho_p$ ) and host fluid ( $\rho_h$ ), gravity ( $g$ ), flake dimension ( $a_j$ ) and the angle of the flake ( $\theta$ ) relative to the electric field [Fig. 118.29(a)]:

$$\Gamma_{Gi} = V_p (\rho_p - \rho_h) g a_j \cos \theta = C_{Gi} \cos \theta. \quad (5)$$

Substituting Eqs. (3)–(5) into Eq. (1) we can solve for the angular velocity of the flake

$$\Omega_i = \frac{d\theta}{dt} = \frac{C_{Ei} \sin \theta \cos \theta - C_{Gi} \cos \theta}{C_{Hi}}. \quad (6)$$

Equation (6) may then be integrated for the time to reorient the PCLC flake from an initial angle  $\theta_0 \sim 0^\circ$  to its final position  $\theta_f \sim 90^\circ$  as

$$\int dt = C_H \int \frac{d\theta}{C_E \sin \theta \cos \theta - C_G \cos \theta} \quad (7)$$

$$t = \frac{C_{Hi}}{C_{Ei}^2 - C_{Gi}^2} \left\{ \begin{aligned} &\left( (C_{Gi} - C_{Ei}) \ln \left[ \cos\left(\frac{\theta}{2}\right) + \sin\left(\frac{\theta}{2}\right) \right] \right)^{\theta_f} \\ &- (C_{Ei} + C_{Gi}) \ln \left[ \cos\left(\frac{\theta}{2}\right) - \sin\left(\frac{\theta}{2}\right) \right] \\ &+ C_{Ei} \ln [C_{Gi} - C_{Ei} \sin(\theta)] \end{aligned} \right\}_{\theta_0}. \quad (8)$$

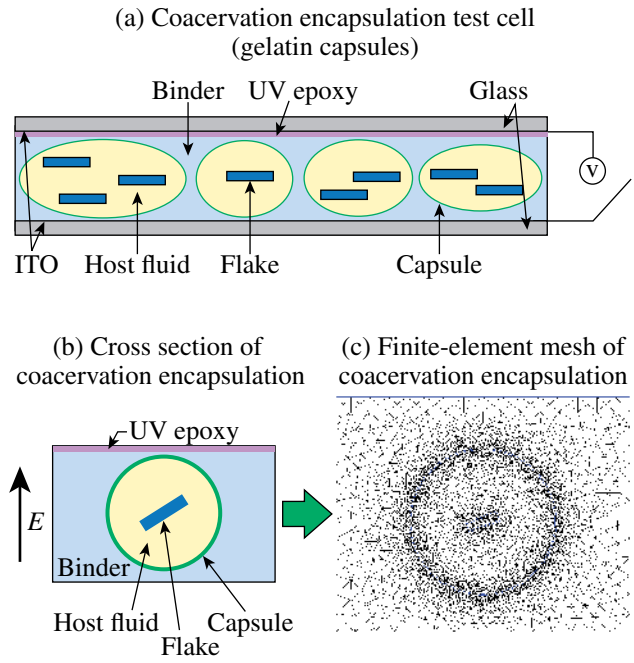
To develop the analytical model shown above, a basic test cell with only a flake/host fluid suspension in the cell gap between the electrodes was studied in previous work to characterize PCLC flake motion in ac and dc electric fields (Fig. 118.29).<sup>7,12–15</sup> This type of cell is used as a baseline for the work reported here.

As the complexity of the cell design increases, the boundary conditions required for an analytical solution make it much more challenging to calculate the electric field applied to the flake. To account for the added boundary conditions created by the microencapsulation of the PCLC flake/host fluid suspension, another method must be found to model the electric field within the test cell. Finite-element-analysis–based software, Comsol Multiphysics (Comsol), offers a straightforward method to account for these boundary conditions in the calculation of the electric field acting on the PCLC flake. The calculation of the electric field combined with the analytical model enables one to predict PCLC flake motion caused by MW polarization in an electric field for complex cell geometries.

Finite-element-analysis–based software was used to analyze the electric field for six types of test cell configurations with three types of host fluids for each configurational variant. The six configurations studied are illustrated in Fig. 118.30. The *basic* cell [Fig. 118.30(a)] with only a flake/host fluid suspension in the cell gap is used as a baseline for our work. The *microwell* cell [Fig. 118.30(b)] adds vertical walls (composed of photoresist) to the cell gap to constrain the flake/host fluid suspension. The fluid is still in contact with the electrodes as in the basic cell and the electric field experiences a *continuous* material path between the electrodes just as in the basic cell. The *microcube* cell [Fig. 118.30(c)] builds on the microwell configuration of Fig. 118.30(b) by adding a layer of photoresist above and below the host fluid that creates a *discontinuous* path for the electric field between the electrodes. For *direct encap-*

sulation cells, two possible methods of assembly are shown. *Direct encapsulation type I* [Fig. 118.30(d)] has the flake/host fluid constrained in a capsule. The path for the electric field is both discontinuous and nonuniform because the curved edges of the capsule are parts of the path between the electrodes. This configuration also includes a layer of epoxy adhesive used for assembly between the binder layer and the top electrode. *Direct encapsulation type II* [Fig. 118.30(e)] also has the flake/host fluid suspension constrained in a capsule similar to type I except there is no adhesive layer between the binder layer and top electrode. Finally, the *coacervation* cell [Fig. 118.30(f)] represents a device that, once assembled, is very similar to the direct encapsulation devices. Here there is an additional discontinuous material forming a separate capsule shell that further complicates the path of the electric field.

The different encapsulation types are intended to show an evolution of complexity in moving from a test cell with only a flake/host fluid suspension in an applied electric field to a flake/host fluid suspension microencapsulated within discrete gelatin capsules. Figure 118.31(a) illustrates a coacervation-type test cell (gelatin capsules) used for electro-optic characterization; the gelatin capsules have been dispersed into a separate film-forming polymer binder, coated onto an indium tin oxide (ITO)-coated substrate and then attached to a second substrate with a UV-cured epoxy. Figure 118.31(b) represents a 2-D cross section of the cell to be modeled. Figure 118.31(c) is

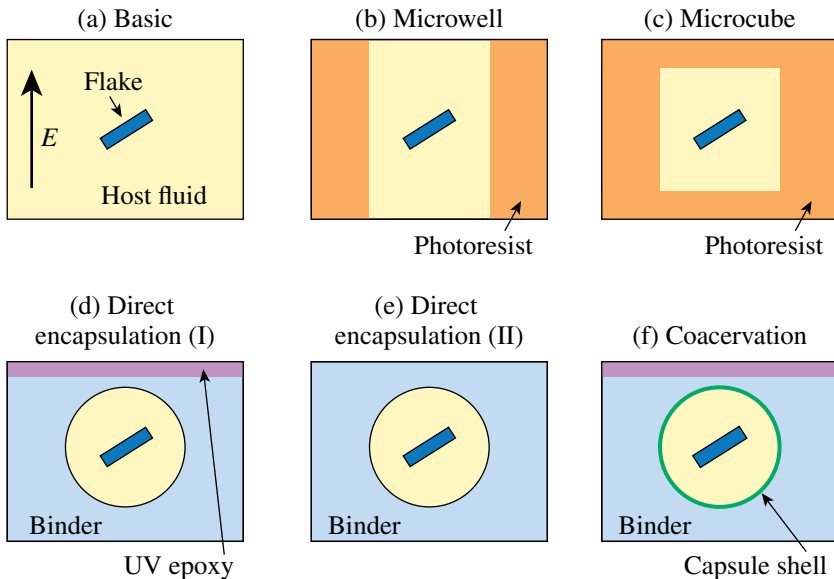


G8685JR

Figure 118.31

(a) Illustrated cross section of a gelatin-gum arabic microcapsule test cell, a more-complex version of the configuration shown in Fig. 118.29 that is based on Fig. 118.30(f); (b) the equivalent cross section for analysis with fluid, flake, gelatin-gum arabic capsule, UV epoxy and polymer binder boundaries in the cell gap; (c) finite-element mesh of the coacervation test cell cross section generated with Comsol Multiphysics.

Test Cell Configurations



G8684JR

Figure 118.30

Six configurations of PCLC flake test cells studied. (a) Basic cell: Contains only a flake/host fluid suspension in the cell gap. (b) Microwell: Insulative vertical walls (photoresist) confine the flake/host fluid suspension within the well; fluid is in contact with electrodes. (c) Microcube: The cube (photoresist) fully encapsulates the flake/host fluid suspension; fluid is not in contact with electrodes. (d) Direct encapsulation (I): A polymer binder (capsule) fully encapsulates the flake/host fluid suspension. The fluid is not in contact with the electrodes, and there is an epoxy layer between the polymer binder and the top electrode. (e) Direct encapsulation (II): The polymer binder (capsule) fully encapsulates the flake/host fluid suspension. The fluid is not in contact with electrodes and there is no epoxy layer between polymer binder and top electrode. (f) Coacervation encapsulation: A polymer binder surrounds a capsule, a thin shell of material different than the binder layer, which fully encapsulates the flake/host fluid suspension. The fluid is not in contact with electrodes and there is an epoxy layer between the polymer binder and the top electrode.

the matching finite-element mesh generated within Comsol, using the “In-Plane Electric Currents” module to analyze the electric field. The gelatin-type capsule with a UV epoxy layer in this configuration is the most complex material set studied in this work.

To model each of the test configurations, a representative 2-D cross section is generated using the Comsol module. Each sub-domain (geometric section) is assigned a value for conductivity, dielectric constant, and thickness in the  $-x$  direction (into the plane of the page, as shown in Fig. 118.29). The glass substrates and ITO layers are not included in the model. An ac voltage ( $7.5 V_{\text{rms}}$  unless noted) is applied to the lower boundary (electrode) of the model and the top boundary (electrode) is set to ground potential. The side boundaries are defined as electrically insulating. The ac frequency is set at 100 Hz and the overall cell gap is  $150 \mu\text{m}$  unless noted other-wise. The flake angle, with respect to the electrode, is fixed at  $20^\circ$  to calculate the electric field for all configurations. The critical cell dimensions, materials, and their properties used in each configuration are listed in Tables 118.II and 118.III. The flake dimensions are as shown in Fig. 118.29(a). For direct comparison of microencapsulation effects on the electric field, only the materials’ properties of SU-8 3050 photoresist were used to model photo-

resist as well as binder layers, even though experiments were conducted with binders made from SU-8 3050, SU-8 2015, PVA (polyvinyl alcohol), and polydimethylsiloxane (PDMS). All four materials have low conductivity and dielectric constant; using only SU-8 3050 for modeling makes the comparison between microencapsulation types straightforward and does not significantly affect the results.

As shown in Fig. 118.31(c), the model is divided into a continuous mesh of finite elements. Each configuration includes a sub-domain of the host fluid in a  $1\text{-}\mu\text{m}$ -thick area immediately surrounding the flake. The normal component of the electric field  $\left\{ \text{e.g., } E_0 = \text{sqrt} \left[ (E_z)^2 + (E_y)^2 \right] \right\}$  is integrated over this sub-domain to calculate the value of the electric field acting on the flake due to the boundary conditions for each configuration. The analytical model, however, assumes  $E_0 \sim E_z$  because  $E_y$  is perpendicular to the electrodes from which the electric field is applied. For ease of calculation in this work, the normal component is used as a reasonable approximation for  $E_0$  because  $E_z \geq 10 E_y$ , as verified in Comsol over a variety of boundary conditions. For the basic cell, this integration is not necessary because the medium in the cell gap (and thus the electric field) surrounding the flake is homogenous, but this step becomes important when the flakes are encapsulated. Once the electric

Table 118.III: Test cell configuration dimensions and materials used for modeling.

Configuration	Cell gap ( $\mu\text{m}$ )	Wall height ( $\mu\text{m}$ )	Wall width ( $\mu\text{m}$ )	Top/ bottom thickness ( $\mu\text{m}$ )	Capsule diam ( $\mu\text{m}$ )	Capsule shell thickness ( $\mu\text{m}$ )	Epoxy layer thickness ( $\mu\text{m}$ )	Wall material	Top/ bottom layer material	Binder material	Capsule material
Basic <sup>+++</sup>	150	n/a	n/a	n/a	n/a	n/a	n/a	n/a	n/a	n/a	n/a
Microwell <sup>+++</sup>	150	150	50	n/a	n/a	n/a	n/a	SU-8	n/a	n/a	n/a
Microcube <sup>+++</sup>	150	150	50	20	n/a	n/a	n/a	SU-8	SU-8	n/a	n/a
Direct Encapsulation (I) <sup>++,#</sup>	190	n/a	n/a	n/a	100	n/a	40	n/a	n/a	PVA/ SU-8	n/a
Direct Encapsulation (II) <sup>++,#</sup>	150	n/a	n/a	n/a	100	n/a	n/a	n/a	n/a	PDMS/ SU-8	n/a
Coacervation <sup>++</sup>	190	n/a	n/a	n/a	100	1	40	n/a	n/a	PVA	Gelatin-gum arabic

n/a = not applicable

<sup>+</sup>Propylene carbonate host fluid tested

<sup>++</sup>SIT7757, DMS-E09 host fluids tested

<sup>+++</sup>SIT7757, DMS-E09, propylene carbonate host fluids tested

<sup>#</sup>SU-8 3050 material properties used for modeling to allow one to directly compare microencapsulation types

field acting on the flake has been calculated, this value is input into the analytical model developed previously.<sup>13,15</sup> The analytical model results are then calculated using Mathematica software (Wolfram Research) to evaluate the PCLC flake reorientation times as a function of the electric field's amplitude and frequency and the physical properties of the flake/host fluid system.<sup>13,15</sup>

### 3. Device Preparation

A minimum of two prototype test cells for each of the six configurations shown in Fig. 118.30 were prepared and evaluated for EO flake behavior. Each prototype was similar to the devices shown in Fig. 118.29, but without patterned electrodes. All of the devices were made using rectangular, 3:1-aspect-ratio polysiloxane PCLC flakes [see Fig. 118.29(a)].<sup>2</sup> Sources for all materials and preparation methods for each configuration are identified below.

The PCLC material is a non-crosslinked cyclic polysiloxane (Wacker-Chemie GmbH, Munich, Germany) with a glass transition temperature  $T_g$  between 40°C and 50°C. The PCLC flakes were made by soft lithography using a patterned silicon wafer<sup>24</sup> to make a mold from a two-part PDMS molding formulation.<sup>25</sup> The PCLC material was blade coated into the mold at 195°C (Refs. 2,3).

Propylene carbonate (99.5%, Acros Organics) was used as a host fluid with high dielectric constant and conductivity. DMS-E09 (Geleste) was used as a host fluid with moderate dielectric constant and conductivity. SIT7757 (Geleste) was used as a host fluid with low dielectric constant and conductivity.

Electro-optical test cells were fabricated using 25-mm × 25-mm × 3-mm ITO-coated substrates (Thin Film Devices), cleaned by a detergent wash (Extran MA 02, EMD Chemicals). The basic test cells used 80- $\mu$ m microspheres (Duke Scientific) mixed into EPO-TEK OG 154 UV curing epoxy (Epoxy Technology) to set the test cell's gap spacing. A drop of OG-154 epoxy/microspheres mixture was applied to the corners of the cell, with the substrates offset so that clips could be attached for electrical connection to the cells. The ac voltage was supplied from a Stanford Research function generator, model DS345, and an HP 6827A Bipolar Power Supply/Amplifier. The dc voltage was supplied by a Fluke High Voltage Power Supply model 412B. A Blak Ray Longwave UV lamp, model B 100AP, was used to cure the epoxy at 365 nm. The two outside edges of the cell were sealed with epoxy and cured. The cell was filled with flake/host fluid suspension (~1% flakes) by capillary action and the remaining two edges sealed with epoxy and cured.

Microwell cells were made by spin coating SU-8 3050 photoresist (MicroChem) at 1000 rpm onto ITO-coated substrates. The microwells were photo-patterned into the SU-8 3050 using a chrome mask (Semiconductor/Microsystems Fabrication Laboratory, RIT) and Blak Ray Longwave UV lamp, model B 100AP. The wells were developed and edge bead was removed using a MicroChem Developer Solution. Next, a drop of OG-154 epoxy without microspheres was applied to the corners of the cell. The microwells were filled with a flake/host fluid suspension by flood coating the microwells and using the top substrate to squeeze out the excess flake/host fluid suspension to an unpatterned area. The cell gap is set by the height of the microwells. The substrates were aligned such that the top and bottom substrates were offset so that clips could be attached for electric connection to the cells from the Stanford Research function generator and ac amplifier or dc power supply. The OG 154 epoxy at the corners of the cell was partially cured; then the cell was edge sealed with epoxy and fully cured.

The microcube cells were constructed following the same procedure as the microwell cells except that a 20- $\mu$ m layer of SU-8 2015 photoresist (MicroChem) was spin coated onto the top and bottom substrates and exposed and developed before the microwells were photo-patterned onto the bottom substrate. The assembly procedure for the microcube devices is the same as that for the microwell devices described earlier.

Direct encapsulation cells were made by emulsifying the flake/host fluid suspension (~1% PCLC flakes) into a 20% aqueous solution of 80% hydrolyzed PVA (Aldrich Chemical). Emulsification was accomplished with low shear by adding a total of 1 g of the components into a 4-ml vial and rotating at ~45 rpm for 15 min. A portion of the emulsion, which depends on the size of the substrate to be coated, was then cast by hand onto an ITO-coated substrate and left to dry for 24 h. Once dry, OG142-13 UV epoxy (Epoxy Technology) was applied to the top of the PVA film; the second substrate was then applied and the cell cured with UV light (365 nm).

The complex coacervation cells were made in two steps: (a) the flake/host fluid suspension was microencapsulated by complex coacervation into gelatin-gum arabic capsules; (b) the capsules were dispersed into a polymeric binder and made into a test cell. Microencapsulation was accomplished by emulsifying 3 g of the flake/host fluid suspension into 6 g of a 1% aqueous solution of gum arabic (Aldrich Chemical) at 55°C using a high-shear mixer (IKA Ultra Turrax Tube Disperser, Cole-Parmer Instrument). Then 6 g of a 1% solution of porcine gelatin (Aldrich Chemical) were added and further emulsified,

and the temperature was reduced to 41°C. Next, the emulsion was diluted by the drop-wise addition of 50 g of water. The pH was then reduced to 4 by the drop-wise addition of 30 g of a 0.2% aqueous solution of acetic acid to induce coacervation. Coacervation continued for 30 min and then the batch was cooled to 5°C. Agitation was continued for 40 min and then the hardening agent, 10 g of a 5% aqueous solution of glutaraldehyde, was added drop-wise. Agitation continued for 1 h and then 100 g of a 4% aqueous solution of NaOH was added drop-wise to raise the pH to ~10 and complete the hardening reaction. The batch of finished capsules was then warmed to room temperature, being dispersed with low shear into 1 g of a 20% aqueous solution of PVA. A film of the dispersion was then cast by hand onto an ITO substrate, and the cell was prepared following the same procedure as a direct encapsulation cell.

#### 4. Characterization

Each device was tested within 48 h after assembly to reduce the effect of aging on the test cell. Aging may increase the reorientation time of PCLC flakes if the ITO electrodes are not insulated from the host fluid.<sup>13</sup> The flake motion and response times were characterized by streaming video with time stamping using a Leitz Orthoplan polarizing optical microscope (POM) (Wetzlar, Germany) in reflection mode coupled with a MicroPix C1024 CCD camera and Streampix software (CCD Direct).

Optical images were taken using a Leica DMXR POM (Leica Microsystems) in reflection mode coupled with a Q-Imaging Retiga 4000R Fast camera and QCapture Pro software (Media Cybernetics).

The dielectric properties of each test cell and selected materials were measured using a Solartron 1260 Impedance Gain-Phase Analyzer (Solartron Analytical) and collected with Zplot and Zview (Scribner Associates) PC interface software.

### Results and Discussion

#### 1. Effect of Cell Geometry on the Electric Field

The environment (cell geometry) surrounding the flake has a large effect on flake motion because it can influence the strength of the applied electric field, which is directly proportional to the electrostatic torque applied to the flake. We calculated the effect of the cell geometry (device configuration) on the electric field while keeping the properties of both the fluid and the flake constant. Figure 118.32 shows the Comsol modeling results for four configurations where a PCLC flake is suspended in the high dielectric constant host fluid propylene carbonate (PC) in a 150- $\mu\text{m}$ -thick test cell

with an applied electric potential of 7.5 V<sub>rms</sub>. The material properties of the photoresist SU-8 3050 were used to model the microwell/microcube walls and the direct encapsulation binder to enable one to directly compare the electric fields between the device geometries. The resulting plots of the electric fields are shown as the test cell geometry changes from a basic configuration [Fig. 118.32(a)] to a direct encapsulation type-II cell [Fig. 118.32(d)].

When the path of the electric field between the electrodes encounters constant material properties, as in both the basic and microwell configurations, a strong electric field is present in the cell gap [Figs. 118.32(a) and 118.32(b)]. This is characterized by the dark gray areas throughout most of the cell gap. A slight drop of the electric field in localized areas around the flake is denoted by a light gray. Additionally, if the dielectric constants and conductivities of the host fluid and PCLC flake are very different, the model predicts a high electrostatic torque on the flakes. When the path of the electric field between the electrodes does not encounter constant material properties, as in both the microcube and direct encapsulation type-II configurations [Figs. 118.32(c) and 118.32(d)], the model prediction depends on the material properties of the system. When the electric field passes from a low-dielectric-constant material such as SU-8 3050 ( $\epsilon = 3.2$ ) into a high-dielectric-constant material such as PC ( $\epsilon = 60$ ), the electric field drops off dramatically. This is seen as regions of very dark gray surrounding the flake in the microcube and direct encapsulation type-II examples [Figs. 118.32(c) and 118.32(d)]. In such cases, even when the dielectric constant and conductivity mismatch between PC and PCLC is large, the flake will experience low electric-field strength and therefore low electrostatic torque. This represents a nonfunctional device configuration.

In addition, a distortion in the electric field results as it encounters material composition changes that are non-normal to the direction of the electric-field orientation. This phenomenon is apparent in both the microcube example at the corners of the microcube and the direct encapsulation example near the edges of the capsule wall [Figs. 118.32(c) and 118.32(d)], where the arrows denoting the electric field are at an angle to, rather than perpendicular to, the top electrode.

#### 2. Effect of Host Fluid on the Electric Field

If the cell geometry is held constant and several host fluids are considered, an equally dramatic effect is observed in the effective electric-field strength as it passes from a region of low to high dielectric constant. In Fig. 118.33, from left to right, a microcube cell is shown with the host fluid properties

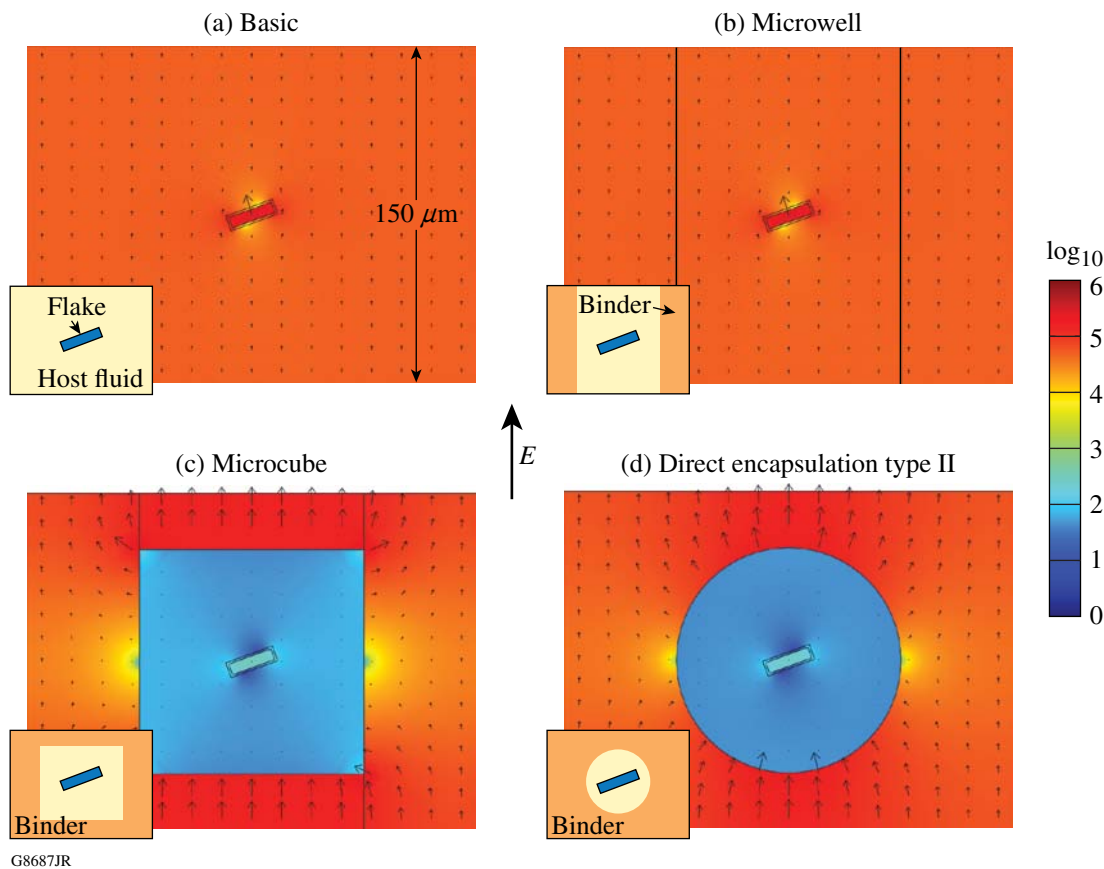


Figure 118.32

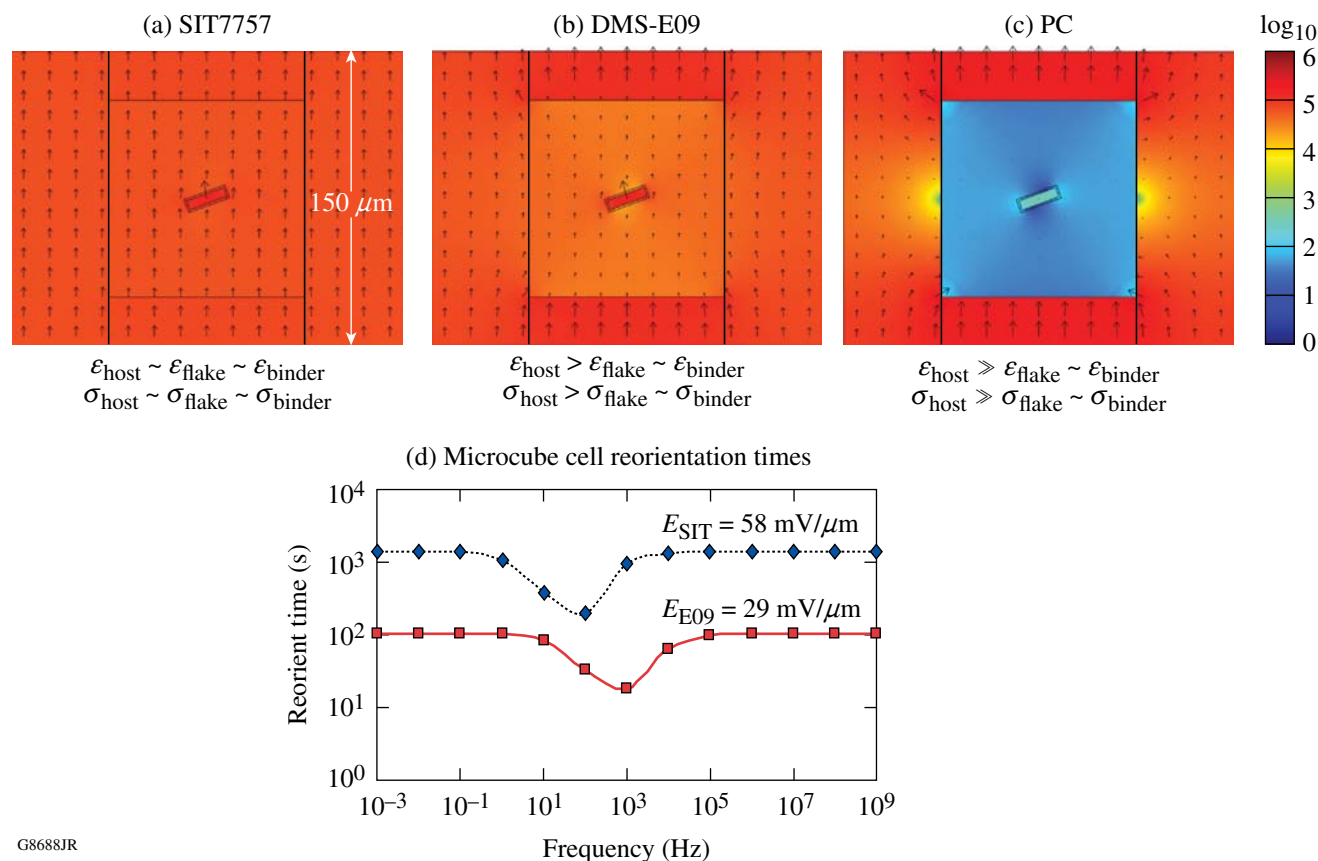
Comsol Multiphysics output of the electric field as a function of test cell geometry (insets highlight geometry). The fluid surrounding the flake has the properties of propylene carbonate ( $\epsilon = 60$ ), the flake is PCLC ( $\epsilon = 2.2$ ), the encapsulating material (binder) is SU-8 3050 ( $\epsilon = 3.2$ ), and the applied voltage to the 150- $\mu\text{m}$ -thick cell is  $7.5 V_{\text{rms}}$ . The direction and size of the arrows represent the direction and strength of the electric field, the surface plot density also represents the strength of the electric field, and the scale range is 0 (black) to  $10^6$  (white) V/m. (a) Basic and (b) microwell configurations have strong uniform electric fields because the materials in the path of the electric fields have uniform dielectric properties. (c) Microcube and (d) direct encapsulation configurations have non-uniform electric fields because materials in the path of the electric fields have dissimilar dielectric properties. Note the electric-field distortion (arrow directions at an angle) near the corners and edges of the microcube and capsule in direct encapsulation.

changing from low  $\epsilon$  and  $\sigma$  [e.g., SIT7757:  $\epsilon = 2.7$ ,  $\sigma = 10^{-8}$ , Fig. 118.33(a)] to moderate  $\epsilon$  and low  $\sigma$  [e.g., DMS-E09:  $\epsilon = 7$ ,  $\sigma = 10^{-8}$ , Fig. 118.33(b)] to high  $\epsilon$  and  $\sigma$  [e.g., PC:  $\epsilon = 60$ ,  $\sigma = 10^{-4}$ , Fig. 118.33(c)]. For all three cells the applied electric potential was  $7.5 V_{\text{rms}}$ , the cell thickness was 150  $\mu\text{m}$ , and the flake angle  $\theta$  was set to  $20^\circ$ . Field strength and, therefore, color within the microcube and adjacent to the flake change from high (light gray) to moderately high (gray) to low (dark gray).

The effect on the magnitude of the electric field combined with the dielectric constant mismatch can be seen in Fig. 118.33(d), where the predicted reorientation times are plotted corresponding to the microcube cells shown in Figs. 118.33(a) and 118.33(b). As seen in Fig. 118.33(d), SIT7757 has a higher electric field acting on the flake, but with a simi-

lar dielectric constant to the flake a longer reorientation time results. Although DMS-E09 has a lower effective electric field, it has a greater difference in dielectric constant with the flake and therefore a faster reorientation time. No curve was plotted for PC as the host fluid in Fig. 118.33(c) because the electric field acting on the flake was so small that no reorientation took place. This is a nonfunctional material combination.

The ac electric field had a range of frequencies over which the induced charge buildup at the flake/host fluid interface caused by MW polarization had the mobility needed to form an induced dipole on the flake. The electric field then acted on the induced dipole to reorient the flake. In Fig. 118.33(d), when the frequency of the electric field was matched to the charge mobility, a minimum reorientation time was achieved. The



G8688JR

Figure 118.33

Electric field as a function of fluid properties in a microcube cell. The direction and size of the arrows represent the direction and strength of the electric field; the surface plot density also represents the strength of the electric field; and the scale range is 0 (black) to 10<sup>6</sup> (white) V/m. (a) Low  $\epsilon$ ,  $\sigma$  (SIT7757), (b) moderate  $\epsilon$ ,  $\sigma$  (DMS-E09), and (c) high  $\epsilon$ ,  $\sigma$  (PC). (d) A corresponding plot of predicted reorientation times for SIT7757 and DMS-E09 with an applied potential of 7.5 V<sub>rms</sub> to a 150-μm-thick cell as a function of ac frequency and type of host fluid. The terms  $E_{SIT}$ ,  $E_{E09}$  are the calculated electric fields acting on the PCLC flake for each host fluid. No curve for PC is shown because  $E_{PC}$  is insufficient to reorient the flake (see text).

particular range of frequencies at which reorientation occurs depends on the composition of the materials system, as seen in Fig. 118.33(d). The SIT 7757 oil has a minimum predicted reorientation frequency of ~200 Hz, while DMS-E09 has a minimum predicted frequency of ~1000 Hz.

Experimental evidence shows that, independent of the host fluid, as reorientation time increases, there is a point at which no physical reorientation will take place. The electrostatic torque on the flake is not enough to overcome counteracting forces such as electrostatic attraction to a surface. Therefore, reorientation will not physically be observed for a PCLC flake in SIT7757 oil, even though a minimum reorientation time of ~120 s is predicted in Fig. 118.33(d). Reorientation of PCLC flakes in DMS-E09 oil, however, is expected near 1000 Hz with response times <60 s.

For PC, the analytical portion of the model predicts an unrealistic *negative*-frequency-independent response for the reorientation time and therefore it is not plotted in Fig. 118.33(d). When the electric field becomes insufficient to reorient the flake, the analytical model will predict a reorientation time <0, indicating flake reorientation in a negative direction (to  $\theta \sim 0^\circ$ ) as a result of the gravitational torque.<sup>13,15</sup>

### 3. Material and Geometry Selection for Increased Electrostatic Torque

Additional modeling was conducted to determine how PCLC flake/host fluid suspensions would behave in microencapsulated geometries resembling electrophoretic (EP)-type devices.<sup>18,19,26,27</sup> Figure 118.34(a) shows a direct encapsulation type-II cell configuration resembling a typical EP device that consists of a PCLC flake in a low-dielectric-constant

fluid that has been encapsulated into a low-dielectric-constant film-forming binder. The resulting high electric field is nearly uniform because the dielectric constants and conductivities of all components are similar. For an EP device, a system with low dielectric constants and conductivities is ideal. For a PCLC flake device, however, both high electric-field penetration and dielectric mismatch of the fluid and particle are needed for MW reorientation to occur. Therefore, the device pictured in Fig. 118.34(a) is nonfunctional.

One obvious way to achieve high electrostatic torque in a direct encapsulation type-II configuration is to microencapsulate a low-dielectric-constant PCLC flake and a moderate-dielectric-constant host fluid within a film-forming binder with a moderate dielectric constant, as shown in Fig. 118.34(b). The slightly darker gray region within the capsule and adjacent to the flake denotes a high electric-field strength. The strong electric field combined with the mismatch in dielectric constant between the flake and the host fluid leads to a functional,

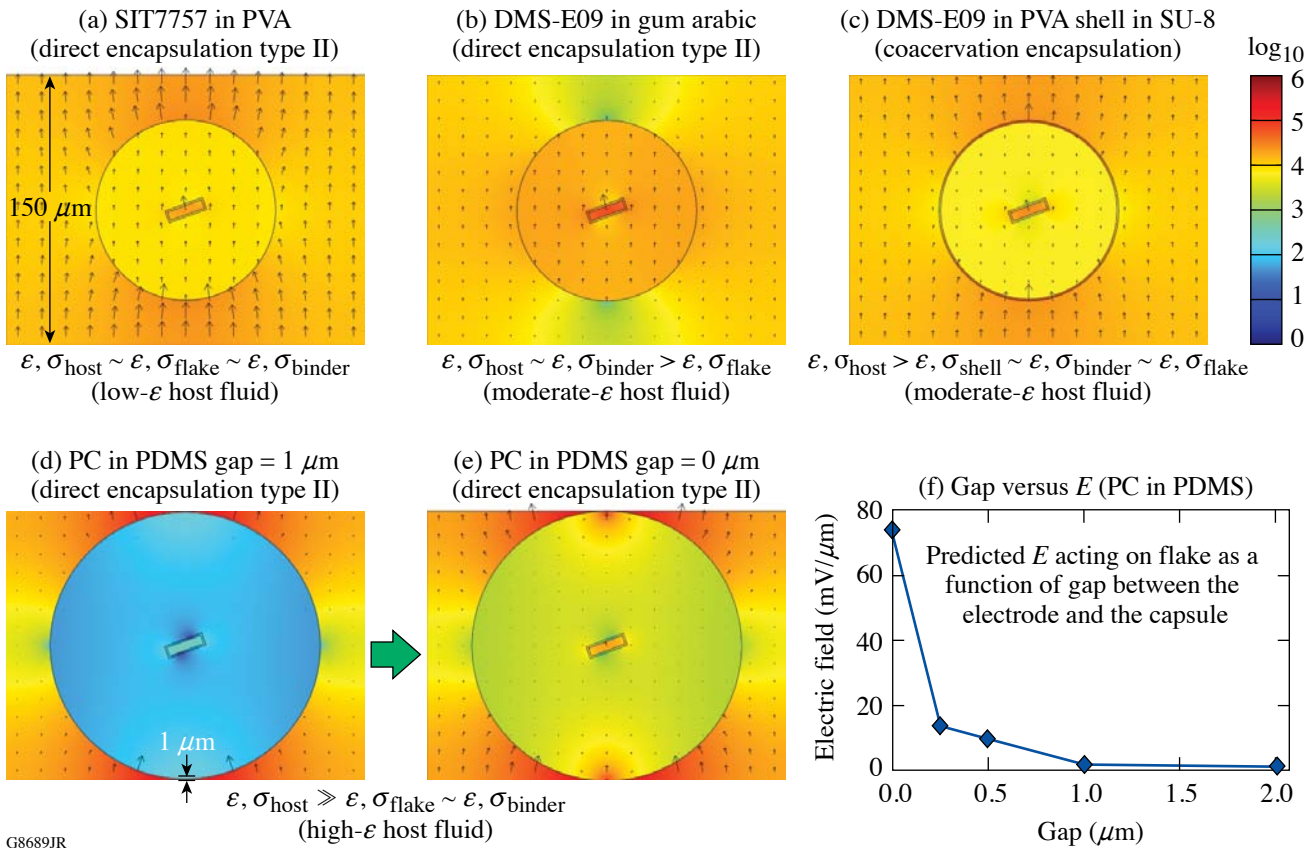


Figure 118.34

Material and geometry effects of microencapsulation on the electric field at an applied potential of  $7.5 V_{\text{rms}}$  for a  $150\text{-}\mu\text{m}$  cell gap. The bar scale for the electric field's magnitude on all plots has a range of 0 (black) to  $10^6$  (white) V/m. (a) PCLC flake suspended in a low-dielectric-constant host fluid encapsulated in a low-dielectric-constant binder (e.g., SIT7757 in PVA) shows high electric-field magnitude in the host fluid. (b) PCLC flake suspended in a moderate-dielectric-constant host fluid encapsulated in a moderate-dielectric-constant binder (e.g., DMS-E09 in Gum Arabic) shows high electric-field magnitude in the host fluid. (c) PCLC flake suspended in a moderate-dielectric-constant host fluid encapsulated in a low-dielectric-constant capsule, with a  $1\text{-}\mu\text{m}$ -thick wall, dispersed in a moderate-dielectric-constant binder (e.g., DMS-E09 encapsulated in a PVA capsule dispersed in a SU-8 3050 binder) shows high electric-field magnitude in the host fluid. (d) PCLC flake suspended in a high-dielectric-constant host fluid directly encapsulated in a low-dielectric-constant binder (e.g., PC emulsified into a PDMS binder) with a  $1\text{-}\mu\text{m}$  gap between the electrodes and capsule wall shows low electric-field strength in the host fluid. (e) PC emulsified into a PDMS binder, as in (d), but now the capsule bridges the gap between the electrodes, resulting in a moderate electric-field magnitude in the host fluid. (f) Plot showing the increase in electric-field magnitude as the gap between the capsule wall and electrode decreases. The difference in the plots of electric-field strength for (a), (b), and (c) is caused by material changes only.

MW-driven PCLC flake device. The distortion of the electric field near the poles [i.e., darker areas above and below the capsules shown in Fig. 118.34(b)] is caused by abrupt changes in dielectric properties along the path of the electric field between electrodes. At the capsule's closest point to the electrodes, the electric-field lines are perpendicular to the capsule and the change in the electric field is the greatest.

An added level of sophistication that would improve process flexibility is to encapsulate the flake/host fluid suspension in a capsule shell of a different material than that of the binder prior to dispersing into a film-forming binder. Such a system would create a greater choice in polymer binders. Concerns such as poor capsule formation caused by miscibility of the host fluid in the binder or a wide distribution of capsule sizes present because of nonuniform mixing, are no longer an issue because the capsules are created in a prior process. Figure 118.34(c) shows this type of configuration (coacervation encapsulation) with the flake/host fluid suspension encapsulated in a capsule shell composed of PVA. For the material set indicated, the polymer binder (SU-8 3050) and host fluid (DMS-E09) are miscible with each other and require the flake/host fluid suspension to be encapsulated before being dispersed in the polymer binder. In Fig. 118.34(c), this material combination is shown to give a moderately high electric field acting on the flake. As in previous examples, care must be taken when selecting materials. If a capsule shell with too high a dielectric constant is used, it will shield the host fluid and flake from the electric field and result in a nonfunctional device. A further level of sophistication can also be added to customize the capsule shells; additives may be incorporated to promote flake bistability or charge control.

Another less-obvious way to make a functional device is to use an approach that is similar to the nonfunctional direct encapsulation type-II configuration in Fig. 118.32(d). A host fluid with higher dielectric constant (PC) can be directly encapsulated into an immiscible low-dielectric-constant binder (PDMS) and still result in a functional device if the gap between the electrode and capsule wall is very small ( $<1 \mu\text{m}$ ). As seen in the transition from Figs. 118.34(d) to 118.34(e), the electric field can be greatly enhanced within the host fluid if the capsule is in contact with the cell electrode. As shown by the plot in Fig. 118.34(f), the greater the portion of the cell gap that is filled by the capsule, the higher the magnitude of the electric field acting on the PCLC flake. A gap of  $2 \mu\text{m}$  between the capsule and electrodes gives an electric field of  $E = 1 \text{ mV}/\mu\text{m}$ , while a gap of  $0.5 \mu\text{m}$  gives  $E = 15 \text{ mV}/\mu\text{m}$ , and a gap of  $0 \mu\text{m}$  gives  $E = 74 \text{ mV}/\mu\text{m}$ .

#### 4. Maxwell–Wagner Behavior in an ac Electric Field

Each device configuration listed in Table 118.II was tested in both ac and dc fields. Our modeling reported here focuses on flake reorientation caused by MW behavior in an ac electric field. As predicted by the modeling work shown in Fig. 118.32 with PC as the host fluid, MW reorientation behavior was observed in basic [Fig. 118.32(a)] and microwell [Fig. 118.32(b)] configurations, but not in microcube [Fig. 118.32(c)] and direct encapsulation type-II [Fig. 118.32(d)] configurations. No MW reorientation is either predicted theoretically or observed experimentally for any configuration when SIT7757 is used as the host fluid for PCLC flakes. Maxwell–Wagner reorientation behavior is both predicted and observed with all six types of encapsulation geometries shown in Fig. 118.30 when DMS-E09 is used as the host fluid. The moderate dielectric constant of the host fluid permits a significant electric field within the host fluid for all configurations while still providing a reasonable difference in dielectric constants when compared to the PCLC flake. This balance of dielectric constants in the cell gap makes it possible for MW polarization-induced effects to occur for all geometries.

To illustrate the effectiveness of our modeling method, the predicted and observed reorientation times as a function of frequency and geometry for DMS-E09 are compared in Fig. 118.35. Cell types with the host fluid in contact with the ITO layer [e.g., basic, microwells, Figs. 118.35(a) and 118.35(b)] show a wide frequency range for the minimum MW reorientation time in ac electric fields, even extending into the mHz (millihertz) regime. Cell types where DMS-E09 is insulated from the ITO layer [e.g., microcubes and direct encapsulation type II, Figs. 118.35(c) and 118.35(d)] show MW reorientation in the ac regime and have a minimum reorientation time at a higher frequency than predicted. When the flake/host fluid suspension is in contact with the ITO layer, ions have been shown to diffuse out of the ITO and increase the conductivity of the test cell.<sup>13</sup> In a basic cell type, with a host fluid having a high dielectric constant (e.g., PC), the increased ion concentration from the ITO lowers the frequency for the minimum reorientation time. As shown in Fig. 118.35, the observed frequency for minimum reorientation times in DMS-E09 are slightly higher than predicted. The difference in frequency ranges over which the two host fluids show MW reorientation behavior is likely caused by the difference in ion mobility between the two fluids (PC:  $\sigma = 10^{-4} \text{ S/m}$ ; DMS-E09:  $\sigma = 10^{-8} \text{ S/m}$ ).

#### 5. Electrophoretic Behavior in a dc Electric Field

Further modifying the analytical portion of the model makes it possible to predict MW flake reorientation in a dc electric field.<sup>14</sup> Additionally, EP translation of low-dielectric-

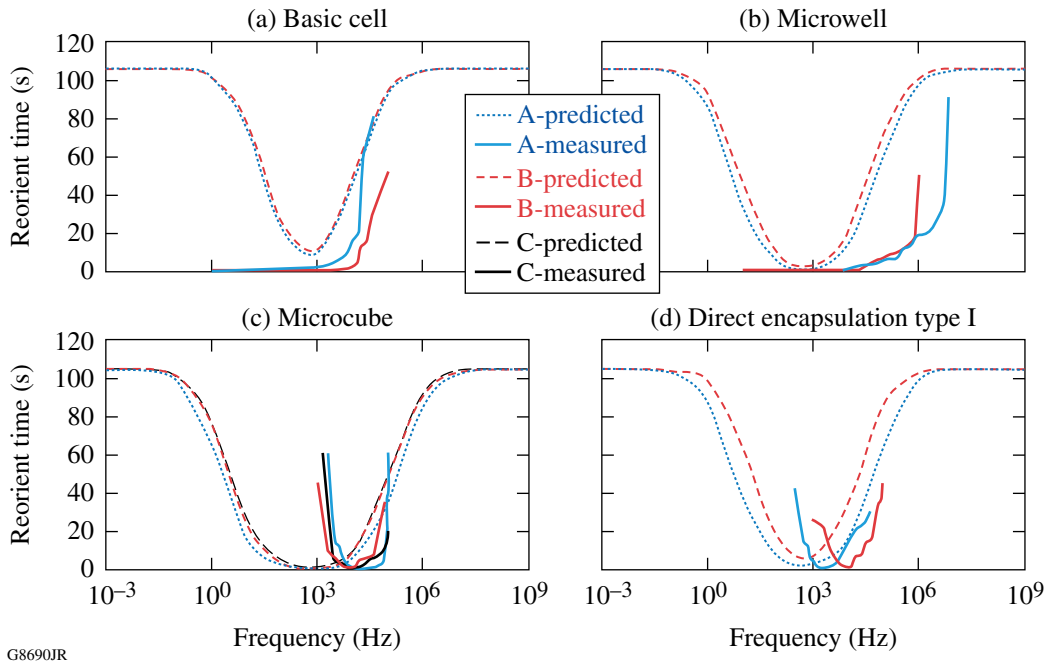


Figure 118.35

Plots of predicted versus observed flake reorientation times in DMS-E09 in an ac electric field: (a) basic, (b) microwell, (c) microcube, and (d) direct-encapsulation, type-I cell types. A, B, and C are individual test cell labels. The differences between predicted and observed values are likely caused by low ion mobility in the DMS-E09 host.

constant PCLC flakes in a dc electric field is also possible. Unfortunately, the analytical portion of the model used here is not applicable to EP motion so no predictive modeling was done. In a dc electric field with SIT7757 as the host fluid, EP motion has been observed for all geometry types. This observation indicates that the flakes have an intrinsic charge in SIT7757. The direction of translation is toward the positive electrode, which implies a negatively charged particle. Figure 118.36 shows the observed translation times as a function of applied voltage for different geometries. All configurations follow the same relationship, with the translation time decreasing with increasing electric-field strength. This behavior is to be expected because the EP force is directly proportional to the effective electric field.<sup>28</sup> Also, all materials in the cell gap (e.g., SIT7757, PVA, SU 8 3050) have low dielectric constants and conductivities. Therefore all configurations have very similar electric-field values acting on the PCLC flakes, and only the minimum voltage for initial translation is different for each configuration. Electrophoretic motion of PCLC flakes in a dc electric field has also been observed in both DMS-E09 and PC as host fluids; however, it is combined with MW reorientation at low electric-field strengths and chaotic electrorotation at higher field strengths.

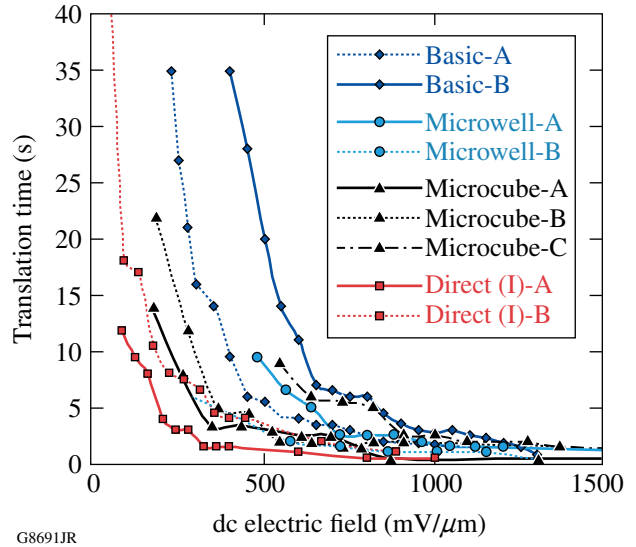


Figure 118.36

Observed PCLC flake electrophoretic translation times in SIT7757 as a function of applied dc electric-field magnitude and test cell geometry. All configurations follow the same relationship, with the translation time decreasing with increasing electric-field strength. A, B, and C are individual test cell labels.

## Conclusions

By using a combination of Comsol Multiphysics and an analytical model developed by our group, we have shown that we can predict both the resultant electric field for any given device geometry and its effect on PCLC flake motion caused by MW interfacial polarization. The effect of the surrounding environment on the PCLC flake's electro-optical behavior depends greatly on both the materials used and the type of microencapsulation geometry. The MW reorientation behavior of PCLC flakes is directly proportional to both the effective electric field acting on the flake and the difference in dielectric constants and conductivities between the host fluid and flake. The optimal cell geometry for MW reorientation will have a balance of uniform dielectric constants and conductivities along the path of the electric field and a mismatch in dielectric constants between the host fluid and flake. With proper matching of device geometry and material properties, we have shown that it is possible to encapsulate a range of host fluids and PCLC flakes while maintaining MW reorientation capability for the flake/host fluid suspension. In addition we have also demonstrated good control over EP-type motion of microencapsulated PCLC flakes in a host fluid with low dielectric constant and conductivity.

The bright reflective colors and inherent circular polarization of PCLC flakes make them promising candidates for switchable reflective particle-based applications, including switchable conformal coatings for micropolarizers, large planar areas, and flexible media for information display applications (e.g., electronic paper). The ability demonstrated in this work to predict the effect of materials' properties and device geometry on the electro-optical behavior of PCLC flake/host fluid suspensions is a critical and significant step forward in the advancement of this unique materials technology toward viable commercial applications.

## ACKNOWLEDGMENT

The authors would like to thank T. Kosc for her assistance and advice with the PCLC flake analytical modeling and interpretation and acknowledge the Laboratory for Laser Energetics at the University of Rochester for continuing support. This research was also supported by the U.S. Department of Energy Office (DOE) of Internal Confinement Fusion under cooperative agreement DE-FC52-08NA28302, the University of Rochester, and the New York State Energy Research and Development Authority. The support of the DOE does not constitute an endorsement by the DOE of views expressed in this article.

## REFERENCES

1. E. M. Korenic, S. D. Jacobs, S. M. Faris, and L. Li, *Mol. Cryst. Liq. Cryst.* **317**, 197 (1998).
2. A. Trajkovska-Petkoska, R. Varshneya, T. Z. Kosc, K. L. Marshall, and S. D. Jacobs, *Adv. Funct. Mater.* **15**, 217 (2004).
3. A. Trajkovska-Petkoska, S. D. Jacobs, T. Z. Kosc, and K. L. Marshall, U.S. Patent No. 7,238,316 (3 July 2007).
4. K. L. Marshall, T. Z. Kosc, A. Trajkovska-Petkoska, E. Kimball, and S. D. Jacobs, presented at the 4th Annual Flexible Microelectronics and Displays Conference, Phoenix, AZ, 1–3 February 2005.
5. K. L. Marshall, K. Hasman, M. Leitch, G. Cox, T. Z. Kosc, A. Trajkovska-Petkoska, and S. D. Jacobs, in *2007 SID International Symposium*, edited by J. Morreale (Society for Information Display, San Jose, CA, 2007), Vol. XXXVIII, Book II, pp. 1741–1744.
6. K. L. Marshall, T. Z. Kosc, S. D. Jacobs, S. M. Faris, and L. Li, U.S. Patent No. 6,665,042 B1 (16 December 2003).
7. T. Z. Kosc, "Motion of Polymer Cholesteric Liquid Crystal Flakes in an Electric Field," Ph.D. thesis, University of Rochester, 2003.
8. T. Z. Kosc, K. L. Marshall, S. D. Jacobs, J. C. Lambropoulos, and S. M. Faris, *Appl. Opt.* **41**, 5362 (2002).
9. T. Z. Kosc, K. L. Marshall, and S. D. Jacobs, U.S. Patent No. 6,829,075 B1 (20 May 2003).
10. T. Z. Kosc, K. L. Marshall, and S. D. Jacobs, U.S. Patent No. 7,042,617 (9 May 2006).
11. K. L. Marshall, E. Kimball, S. McNamara, T. Z. Kosc, A. Trajkovska-Petkoska, and S. D. Jacobs, in *Liquid Crystals VIII*, edited by I.-C. Khoo (SPIE, Bellingham, WA, 2004), Vol. 5518, pp. 170–181.
12. T. Z. Kosc, K. L. Marshall, S. D. Jacobs, and J. C. Lambropoulos, *J. Appl. Phys.* **98**, 013509 (2005).
13. A. Trajkovska-Petkoska, "Enhanced Electro-Optic Reorientation of Polymeric Cholesteric Liquid Crystal Flakes in Host Fluids," Ph.D. thesis, University of Rochester, 2007.
14. A. Trajkovska Petkoska, T. Z. Kosc, K. L. Marshall, K. Hasman, and S. D. Jacobs, *J. Appl. Phys.* **103**, 094907 (2008).
15. T. Z. Kosc, A. Trajkovska Petkoska, J. C. Lambropoulos, K. L. Marshall, and S. D. Jacobs, "Extended Model for Polymer Cholesteric Liquid Crystal Flake Reorientation and Relaxation," submitted to the *Journal of Applied Physics*.
16. E Ink Corp. Product Page, Electronic Paper Displays, E Ink Corporation, Cambridge, MA 02138.
17. Y. Chen *et al.*, *Nature* **423**, 136 (2003).
18. B. Comiskey *et al.*, *Nature* **394**, 253 (1998).
19. H. L. Guo and X. P. Zhao, *Opt. Mater.* **26**, 297 (2004).
20. I. Shiyanovskaya *et al.*, in *2005 SID International Symposium*, edited by J. Morreale, Digest of Technical Papers, 1st ed. (Society for Information Display, San Jose, CA, 2005), Vol. XXXVI, Book II, pp. 1556–1559.
21. S. W. Stephenson *et al.*, in *2004 SID International Symposium*, edited by J. Morreale, Digest of Technical Papers, 1st ed. (Society for Information Display, San Jose, CA, 2004), Vol. XXVIII, Book II, pp. 774–777.

22. J. Szep, Computerworld – Mobile & Wireless (5 April 2007).
23. T. Z. Kosc, Opt. Photonics News **16**, 18 (2005).
24. Semiconductor & Microsystems Fabrication Laboratory, Kate Gleason College of Engineering, Rochester Institute of Technology, Rochester, NY 14623-5603.
25. Sylgard 184, Dow Corning Corporation, Midland, MI 48686-0994.
26. J. K. Song, H. J. Choi, and I. Chin, J. Microencapsul. **24**, 11 (2007).
27. J. K. Song *et al.*, Mol. Cryst. Liq. Cryst. **464**, 263 (2007).
28. I. D. Morrison and S. Ross, *Colloidal Dispersions: Suspensions, Emulsions, and Foams* (Wiley-Interscience, New York, 2002).